# An oncolytic vaccinia virus expressing anti-CD47 nanobody exerts enhanced antitumor activity by mediating innate and adaptive immune cell infiltration and activation in the lymphoma tumor microenvironment

Mengyuan Li,[1*] Yinyin Zhang,[1*] Lihong Zong,[1*] Minghuan Zhang,[1] Shibing Wang,[2] Wen Lei[1,3] and Wenbin Qian[1,3,4]

[1]Department of Hematology, the Second Affiliated Hospital, College of Medicine, Zhejiang University; [2]Department of Clinical Laboratory, Affiliated Hangzhou First People's Hospital, School of Medicine, Westlake University; [3]Key Laboratory of Cancer Prevention and Intervention, China National Ministry of Education, Zhejiang Provincial Clinical Research Center for Cancer, Cancer Center of Zhejiang University, the Second Affiliated Hospital, College of Medicine, Zhejiang University and [4]Research Center for Life Science and Human Health, Binjiang Institute of Zhejiang University, Hangzhou, China

*ML, YZ and LZ contributed equally as first authors.*

**Correspondence:** W. Qian
qianwb@zju.edu.cn

W. Lei
leiwen2017@zju.edu.cn

**Received:** November 14, 2024.
**Accepted:** April 3, 2025.
**Early view:** April 10, 2025.

**https://doi.org/10.3324/haematol.2024.286923**



## Abstract

Anti-CD47 antibodies targeting macrophage immune checkpoints have demonstrated benefit in clinical trials, particularly in combination with targeted therapies. Nevertheless, this strategy faces challenges from suboptimal efficacy and on-target toxicity due to an immunosuppressive tumor microenvironment and ubiquitous CD47 expression. Here, we report a novel oncolytic vaccine virus (OVV) that expresses therapeutic transgenes encoding an anti-mouse CD47 nanobody or an anti-human CD47 nanobody fused with the IgG1 Fc fragment (termed OVV-mCD47nb and OVV-hCD47nb-G1, respectively), and show that anti-CD47 nanobodies secreted by lymphoma cells infected with armed OVV enhanced tumor phagocytosis via blockade of the CD47/SIRPα signal pathway. In an implanted subcutaneous lymphoma mouse model, OVV-mCD47nb demonstrated superior therapeutic efficacy and significantly prolonged survival of tumor-bearing mice when compared to its parental OVV, an effect which might be associated with the recruitment and activation of macrophages, natural killer cells, and T cells within the tumor microenvironment. Importantly, we discovered that the specific binding of secreted hCD47nb-G1 to CD47 enhanced macrophage-mediated tumor cell phagocytosis while sparing red blood cells. OVV-hCD47nb-G1 demonstrated superior antitumor efficacy compared to the anti-CD47 antibody Hu5F9 in lymphoma models. Both intratumoral and intraperitoneal administration of OVV-hCD47nb-G1 achieved significant tumor regression and prolonged survival, potentially through tumor microenvironment reprogramming via enhanced immune cell activation. Notably, combination with CD19 chimeric antigen receptor T cells synergistically improved therapeutic outcomes in subcutaneous lymphomas by overcoming the critical barrier of limited chimeric antigen receptor T-cell infiltration. Our findings establish that arming OVV with a CD47-blocking nanobody and IgG1 Fc creates a dual-functional therapeutic platform, offering a paradigm-shifting strategy for lymphoma immunotherapy through coordinated innate and adaptive immune activation.

## Introduction

Diffuse large B-cell lymphoma (DLBCL) is the most common subtype of non-Hodgkin lymphoma.[1] Patients with relapsed/refractory DLBCL face dismal outcomes, with a median overall survival of 6.3 months after conventional treatments.[2] Recently, chimeric antigen receptor (CAR) T-cell therapy, one of the most successful cell therapies, demonstrated substantial efficacy in DLBCL patients. However, the majority of patients relapsed even after achieving remission or became refractory to treatment.[3-5] Therefore, there still exists a highly unmet need for a novel therapeutic strategy.

The field of immunotherapies is evolving rapidly and has

significantly impacted outcomes in lymphoma. However, immunotherapy studies on lymphomas often target immune checkpoints related to adoptive immunity.[6] Innate immune checkpoints, such as the CD47/signal regulatory protein α (SIRPα) pathway, also play a critical role in tumor-mediated immune escape, thereby representing potential targets for cancer immunotherapy.[7] CD47 is upregulated in DLBCL and is strongly associated with tumor progression, treatment resistance, and adverse clinical outcomes.[8-11] Targeting the CD47/SIRPα axis using blocking antibodies is currently under investigation in clinical trials across several hematologic tumors.[12-14] In relapsed/refractory DLBCL, the CD47-blocking antibody Hu5F9-G4 (magrolimab) combined with rituximab is demonstrating promising efficacy, however, significant challenges persist, including treatment-related toxicities and the immunosuppressive tumor microenvironment that limits therapeutic responses.[12,13]

Recent advancements in innovative strategies – such as structural optimization of anti-CD47 antibodies, localized intratumoral delivery systems, and novel combination therapies – have significantly improved the safety, efficacy, and clinical applicability of CD47-targeted therapies.[12,15] Oncolytic viruses selectively target malignant cells, enhance antigen presentation, activate antitumor immune responses, and reprogram the immunosuppressive tumor microenvironment.[16-18] Furthermore, oncolytic viruses have been validated as versatile delivery platforms capable of tumor-specific payload transport, thereby amplifying local immune activation while minimizing systemic toxicity.[16,19-21]

In this study, we engineered a novel oncolytic vaccine virus (OVV) for DLBCL therapy by arming oncolytic viruses with either anti-mouse CD47 nanobody (OVV-mCD47nb) or an anti-human CD47 nanobody fused with the IgG1 Fc fragment (OVV-hCD47nb-G1) for preclinical evaluation. Anti-CD47 nanobodies secreted by lymphoma cells infected with armed OVV enhanced tumor phagocytosis. In a subcutaneous lymphoma mouse model, compared to its parental OVV, OVV-mCD47nb significantly prolonged survival of tumor-bearing mice, which might be associated with the recruitment and activation of macrophages, natural killer (NK) cells, and T cells. Specifically, we discovered that the binding of secreted hCD47nb-G1 to CD47 enhanced macrophage-mediated tumor cell phagocytosis while sparing red blood cells. Administration of OVV-hCD47nb-G1 via intratumoral or intraperitoneal routes demonstrated potent antitumor efficacy in lymphoma models, significantly suppressing tumor burden and extending overall survival. Moreover, combination with CD19 CAR T cells synergistically improved therapeutic outcomes in subcutaneous lymphomas by overcoming the critical barrier of limited CAR T-cell infiltration. These findings underscore its potential as a novel combinatorial immunotherapy that synergizes oncolytic activity with CD47 blockade to enhance macrophage-mediated phagocytosis.

# Methods

## Preparation of the recombinant oncolytic viruses

The control OVV was described previously.[21] A DNA fragment encoding mouse anti-CD47 nanobody was synthesized (GenScript, Nanjing, China) and subcloned into the shuttle plasmid pVV-Control, creating the recombinant plasmid pVV-mCD47nb. This vector contains a synthesized early/later promoter (pse/L) that drives the expression of mCD47nb, a p7.5K early/later promoter that drives the expression of enhanced green fluorescent protein (reporter gene), and guanine-hypoxanthine phosphoribosyl transferase (screening gene). Western reserve strain of vaccinia virus (WR-VV; Cat# VR-1354; ATCC) was used as a backbone virus to generate the VV thymidine kinase gene deletion mutants via homologous recombination.

To synthesize human CD47 nanobody, a phage display library of variable heavy-chain domain of heavy-chain antibody phages was developed by quantitative reverse transcription polymerase chain reaction from mRNA isolated from the peripheral blood lymphocytes of a vaccinated alpaca. The human CD47 antigen-specific nanobodies were screened by enzyme-linked immunosorbent assays. Then the nanobody sequence was cloned in the pVV-Control vector. Virus propagation and titration were performed using HeLa-S3 and HEK293 cells, respectively.

## Animal experiments

All animal studies were approved by the Ethics Committee for Animal Experimentation of the Second Affiliated Hospital of Zhejiang University. Female, 8-week-old, BALB/C mice, NOD/ShiLtGpt-Prkdc$^{em26cd52}$Il2rg$^{em26cd22}$/Gpt (NSG) mice and CB17.SCID (SCID) mice were used in this study. A20 cells ($5\times10^6$) were subcutaneously injected into the right flank of BALB/C mice, and tumor size was measured. The tumor volume was calculated as follows: length × width$^2$ × 0.5. When the tumor volume reached approximately 100 mm$^3$, mice were randomly assigned to receive phosphate-buffered saline (PBS), OVV, or OVV-mCD47nb. To assess immune cell infiltration and bystander effects during virotherapy, Raji cells were injected into the right flank of SCID and NSG mice. After 5 days, when tumors reached ~75 mm$^3$, Raji cells were also injected into the left flank of SCID mice. These mice received weekly intratumoral injections of PBS, OVV, and OVV-hCD47nb-G1 ($1\times10^8$ plaque-forming units [PFU]) for 3 weeks. Tumors were collected for analysis 48 hours after the second treatment, and blood samples were taken after the third treatment. NSG mice received $1\times10^7$ CD19 CAR T cells intravenously following one intratumoral injection of the OVV-hCD47nb-G1.

We established a systemic tumor model using NSG mice via intravenous injection of $1\times10^5$ luciferase-expressing Raji cells (Raji-luc). On day 5, mice received intraperitoneal injections of PBS, OVV, and OVV-hCD47nb-G1 ($1\times10^7$ PFU) and Hu5F9-G4 (200 μg per mouse daily for 1 week). Tumor

growth was monitored by bioluminescence imaging using an IVIS Lumina XRMS Imaging System (PerkinElmer). After 2 days of treatment, peripheral blood and plasma were collected to measure chemokine levels using Luminex Mouse Cytokine 31-plex (Univ-bio, Shanghai, China).

### Statistical analysis

GraphPad Prism (GraphPad Software 8.3.0, Inc.) was used for statistical analysis. Continuous data are given as means ± standard deviation and were compared through unpaired two-tailed Student's *t* tests and analysis of variance. The survival curve was determined by the Kaplan-Meier method. *P* values <0.05 are considered statistically significant. Additional methods used in this study are described in the *Online Supplementary Methods*.

## Results

### High expression of CD47 protein predicts survival of patients with diffuse large B-cell lymphoma treated with CD19-specific chimeric antigen receptor T cells, but not of those treated with immunochemotherapy

CD47 transcript and protein expression are aberrantly upregulated, an effect that was predictive of survival and refractoriness to treatment in DLBCL.[8-11] In this study, we performed immunohistochemical assays including CD47, CD20, and CD3 in newly diagnosed or relapsed/refractory DLBCL patients who received CD19-specific CAR T-cell treatment (for the patients' characteristics, see *Online Supplementary Table S1*). CD47 staining intensity of tumor cells was classified into five levels, comprising 0, negative; 1, faint; 2, weak; 3, intermediate; 4, strong. Patients who scored 0 to 2 were classified as CD47-low, and those scored 3 to 4 as CD47-high (Figure 1A). In survival analyses of newly diagnosed DLBCL patients treated with immunochemotherapy, no statistically significant difference in overall survival was observed between the CD47-high and CD47-low subgroups (Figure 1B). Interestingly, compared with CD47-high expression, CD47-low expression was significantly correlated with longer overall survival in relapsed/refractory DLBCL patients (median overall survival of 10 months *vs*. not reached; *P*<0.001).

To evaluate the prognostic impact of CD47 expression in germinal center B-cell (N=25) and non-germinal center B-cell (N=42) DLBCL subtypes, we compared overall survival between the CD47-high and CD47-low subgroups. Among patients with the non-germinal center B-cell subtype, CD47-high patients exhibited significantly inferior overall survival compared to their CD47-low counterparts (*P*=0.022). A trend toward inferior overall survival was observed in CD47-high patients, although statistical significance was not reached (Figure 1C). In the cohort that achieved a complete response, CD47-high remained an independent predictor of reduced overall survival (*P*=0.004), whereas among patients who did not have a complete response no survival difference was seen between CD47 expression subgroups (Figure 1D).

### Anti-mouse CD47 nanobody expression does not impair the oncolytic activity of the oncolytic vaccine virus and enables phagocytosis of lymphoma cells

A recombinant OVV-mCD47nb, encoding an anti-mouse CD47 nanobody, was generated (Figure 2A). To assess the impact of the mCD47nb transgene on viral infectivity, we treated A20 cells, which were demonstrated to express a high level of CD47 (*Online Supplementary Figure S1A*), with OVV-mCD47nb or its parental OVV. No significant difference in viral infection was observed (Figure 2B). Additionally, OVV-mCD47nb had similar *in vitro* antilymphoma activity compared to control OVV (Figure 2C). These results are consistent with our previous findings,[21] indicating that the insertion of therapeutic genes does not affect the infective and oncolytic ability of OVV.

To investigate the functionality of secreted mCD47nb protein, we purified it from the supernatants of OVV-mCD47nb-infected A20 cells. We exposed A20 to the purified mCD47nb at different concentrations for 30 minutes and measured mCD47nb binding on the surface of A20 cells using an anti-Flag antibody conjugated with APC. Dose-dependent increased binding of mCD47nb was observed (Figure 2D). Then A20 cells were used as target cells and labeled with CellTracker Green CMFDA in order to evaluate induction of potent macrophage-mediated phagocytosis of lymphoma. The phagocytic activity of murine bone marrow-derived macrophages was measured by counting the number of ingested cells using fluorescence-activated cell sorting. Notably, mCD47nb enabled phagocytosis of A20 cells compared to PBS control and the supernatants of OVV (Figure 2E). We also observed that mCD47nb-treated macrophages had upregulated mRNA expression of *Il-1β*, *Il-6*, *Il10*, and *Nos2* (Figure 2F), which are associated with the activation of M1 macrophages.[22-24]

### OVV-mCD47nb induces enhanced antitumor activity in a xenograft lymphoma mouse model via remodeling of the tumor microenvironment

We next evaluated the *in vivo* antitumor efficacy of OVV-mCD47nb in BALB/c mice, a suitable species for studying immune cells within tumors, bearing subcutaneous A20 lymphoma xenografts. Mice with established tumors (mean volume: 100 $mm^3$) received six doses of OVV or OVV-mCD47nb. OVV-mCD47nb significantly delayed tumor progression and prolonged the survival of mice, which had a median survival time of 64 days (Figure 3A, B). These results indicate the superior treatment efficacy of OVV-mCD47nb over OVV therapy.

We next moved forward to detect the binding mCD47nb on tumor cells obtained from the mice treated with OVV-mCD47nb, demonstrating the presence of binding mCD47nb on tumor cells (Figure 3C). We then analyzed tumor-infiltrating

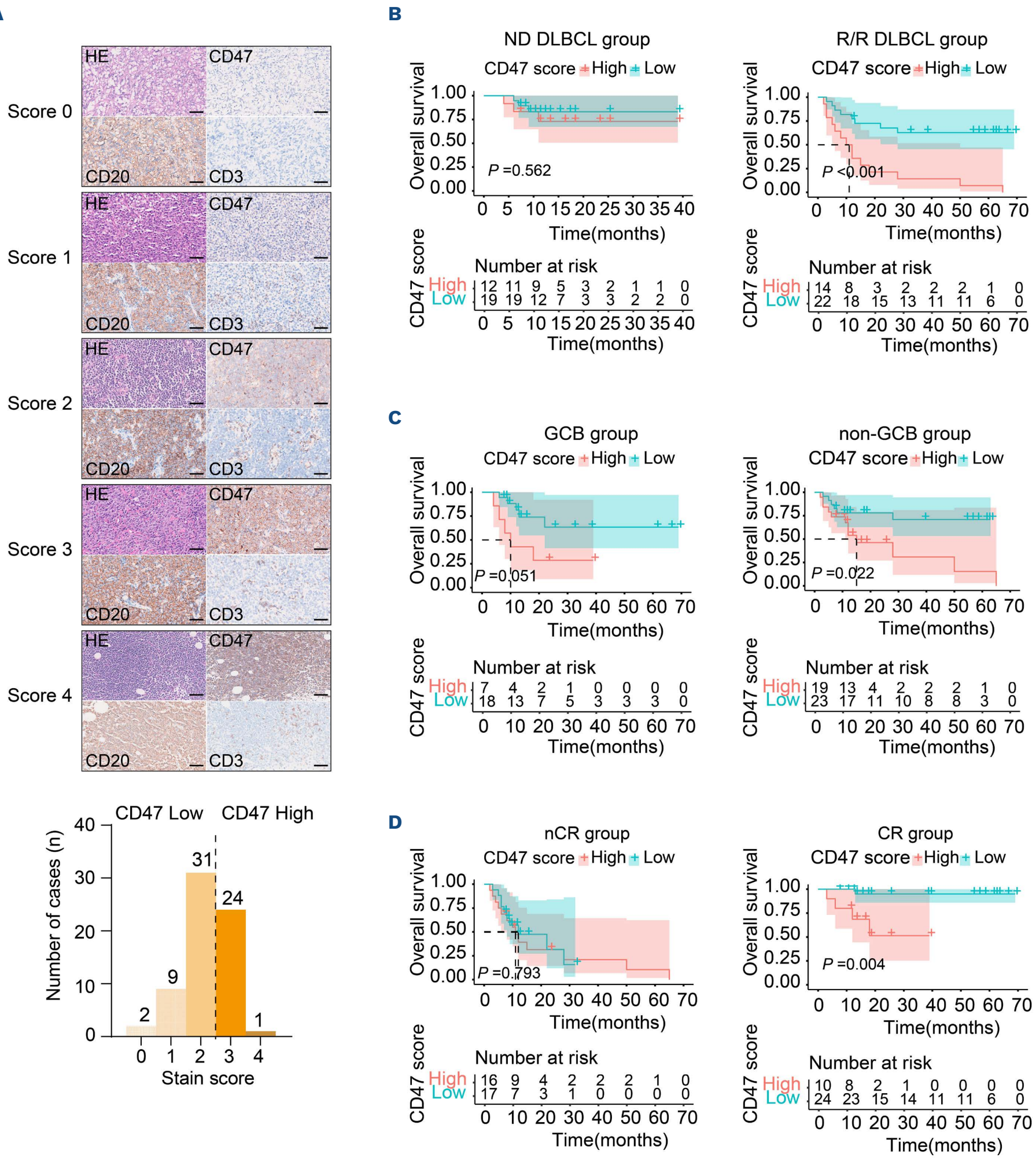


**Figure 1. Protein expression of CD47 in patients with diffuse large B-cell lymphoma was associated with survival.** (A) Top panel. Representative immunohistochemical staining of CD47 protein in tumors of patients with diffuse large B-cell lymphoma. Scale bars, 50 μm. Bottom panel. The levels of CD47 protein expression on the tissue array were classified into CD47-Low (scored as 0~2) and CD47-High (scored as 3~4). (B) Comparison of overall survival between CD47-Low and CD47-High subgroups in patients with newly diagnosed and relapsed/refractory diffuse large B-cell lymphoma. (C) Comparison of overall survival between CD47-Low and CD47-High subgroups in patients with germinal center B-cell lymphoma and the non-germinal center B-cell lymphoma subtype. (D) Comparison of overall survival between CD47-Low and CD47-High subgroups in patients in complete remission and in those not in complete remission. HE: hematoxylin and eosin staining; ND: newly diagnosed; DLBCL: diffuse large B-cell lymphoma; R/R: relapsed/refractory; GCB: germinal center B-cell; nCR: non-complete remission; CR: complete remission.

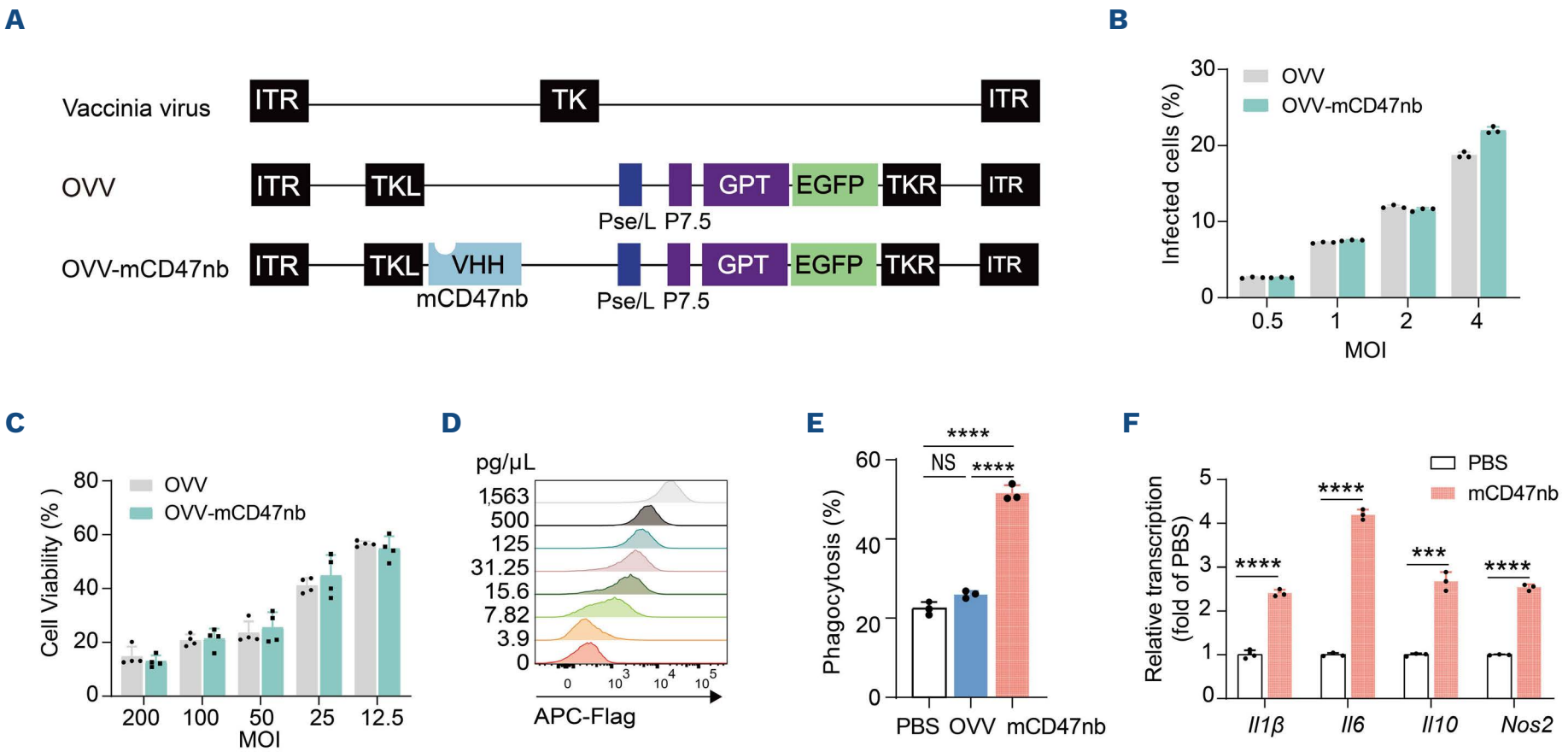


**Figure 2. Construction and oncolytic properties of OVV-mCD47nb *in vitro*.** (A) Schematic structure representation of OVV-mCD47nb, a novel oncolytic vaccine virus (OVV) that expresses transgenes encoding the anti-mouse CD47 nanobody (mCD47nb). Variable heavy-chain domain of heavy-chain antibody domain of anti-mouse CD47 followed by the Flag tag was inserted into the vaccinia virus thymidine kinase gene. (B) Viral infection of OVV-mCD47nb. A20 cells were infected with OVV or OVV-mCD47nb at a multiplicity of infection of 0.5, 1, 2, and 4 for 48 hours. Cells were harvested and analyzed by flow cytometry and the percentage of EGFP$^+$ cells was determined. (C) Cytotoxicity of OVV-mCD47nb and OVV. A20 cells were infected with serial dilutions of oncolytic viruses. Cell viability was measured at 72 hours after infection. (D) Binding ability of mCD47nb to CD47. A20 cells ($1\times10^5$) were co-incubated with variable concentrations of mCD47nb for 30 minutes at room temperature; after washing the cells with phosphate-buffered saline once, they were incubated with APC anti-Flag antibody for 30 minutes followed by flow cytometry analysis. (E) Examination of the effect of mCD47nb purified from oncolytic virus-infected cells on phagocytosis. Bone marrow-derived macrophages stained with red CMTPX were co-cultured with tumor cells stained with green CMFDA. Then CMTPX$^+$CMFDA$^+$ cells were determined by flow cytometry. (F) The mRNA levels of cytokines of bone marrow-derived macrophages were determined by quantitative reverse transcription polymerase chain reaction. OVV: oncolytic vaccine virus; ITR: inverted terminal repeat; TKL: thymidine kinase left homology arm; TKR: thymidine kinase right homology arm; VHH: variable heavy-chain domain of heavy-chain antibody; TK: thymidine kinase; pse/L: synthesized early/later promoter; GPT: guanine-hypoxanthine phosphoribosyl transferase; EGFP: enhanced green fluorescent protein; MOI: multiplicity of infection; PBS: phosphate-buffered saline; NS: not statistically significant.

immune cells 19 days after the first treatment. Increased infiltration of CD45$^+$ immune cells, including elevated proportions of T cells, NK cells, and macrophages, was observed in both the OVV-mCD47nb and OVV treatment groups (Figure 3D). Analyses of T-cell subsets and macrophage polarization in tumor tissues demonstrated that OVV-mCD47nb reduced CD4$^+$ T-cell infiltration while enhancing CD8$^+$ T-cell accumulation. Both OVV-mCD47nb and OVV induced an increase in the number of central memory T cells. Notably, compared to control PBS treatment, both OVV-mCD47nb and OVV treatment significantly increased M1 macrophage infiltration while reducing M2 macrophage accumulation (immunosuppressive/pro-tumor) in tumor tissues (Figure 3E). We further analyzed the activation of immune cells within tumor tissues. As expected, OVV-mCD47nb or OVV intratumoral injection resulted in a significant increase in the percentage of CD69$^+$ NK cells and upregulation of expression of IFN-γ in both T cells and NK cells (Figure 3F).

## Generation and characterization of an armed oncolytic vaccine virus expressing an anti-human CD47 nanobody

To investigate whether this immunovirotherapy provided a compelling advantage for clinical translation, a novel OVV was genetically engineered to express an anti-human CD47 nanobody fused with the IgG1 Fc fragment that enhances antibody-dependent cell-mediated cytotoxicity (Figure 4A). Having demonstrated a high expression of CD47 on four kinds of human B-cell lymphoma cell lines (*Online Supplementary Figure S1B*), we evaluated the infectivity and oncolytic potential of OVV-hCD47nb-G1 and OVV. No difference in viral infectivity was observed, indicating that the insertion of the hCD47nb-G1 gene did not interfere with infection. Both OVV-hCD47nb-G1 and OVV suppressed the viability of all kinds of lymphoma cells in a dose-dependent manner, which seemed to correlate with their infectivity (Figure 4B).

A higher level of hCD47nb-G1 proteins was produced and efficiently released from OVV-hCD47nb-G1-infected lymphoma

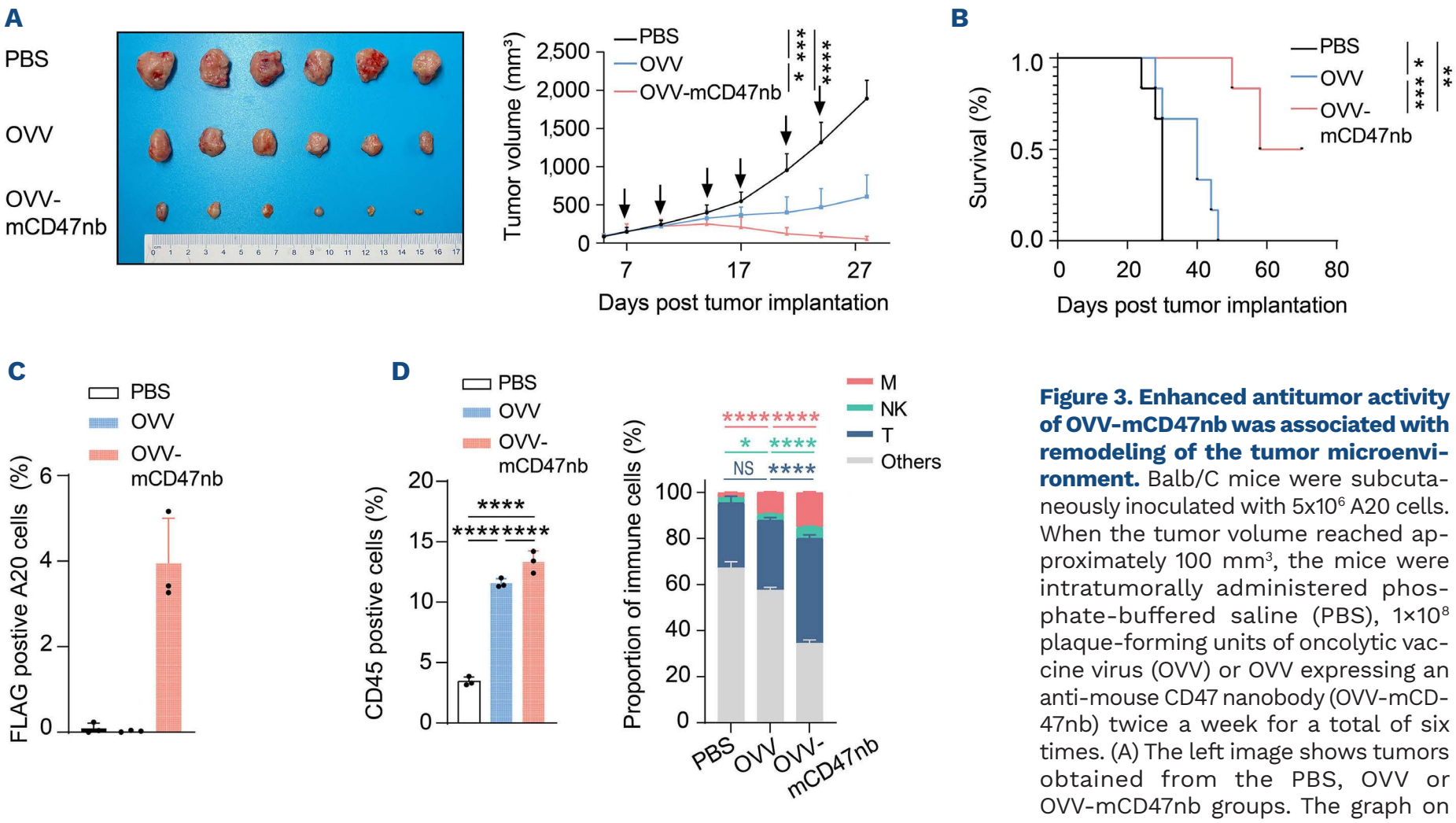


**Figure 3. Enhanced antitumor activity of OVV-mCD47nb was associated with remodeling of the tumor microenvironment.** Balb/C mice were subcutaneously inoculated with $5x10^6$ A20 cells. When the tumor volume reached approximately 100 $mm^3$, the mice were intratumorally administered phosphate-buffered saline (PBS), $1×10^8$ plaque-forming units of oncolytic vaccine virus (OVV) or OVV expressing an anti-mouse CD47 nanobody (OVV-mCD47nb) twice a week for a total of six times. (A) The left image shows tumors obtained from the PBS, OVV or OVV-mCD47nb groups. The graph on the right shows the average tumor volume of lymphoma in mice given the indicated treatments (N=6 for each group). (B) Survival curves of mice treated with OVV or OVV-mCD47nb. PBS was used as a control (N=6 for each group). (C) On day 19, the tumors were excised for analysis. The binding of mCD47nb on the surface of tumor cells was detected by flow cytometry using APC anti-Flag tag antibody (N=3). (D) The tumor-infiltrating $CD45^+$ cells (left) and immune cell subtypes within the $CD45^+$ cells (right) were quantified by flow cytometry (N=3). (E) Left panel. The graph shows the frequency of $CD8^+$, $CD4^+$, and $CD62L^+CD44^+$ T cells within the tumor microenvironment (N=3). Right panel. Graphical representation of the change of M1 and M2 macrophages in the tumors measured (N=3). (F) Percentages of $CD69^+$ natural killer cells and levels of interferon-γ produced by $CD3^+$ T cells and natural killer cells in the tumors, determined using flow cytometry (N=3). Comparisons were made using one-way analysis of variance with Tukey's multiple comparison tests (A) on day 28, (C, D, E, and F) on day 19, and the log-rank (Mantel-Cox) test (B). All data are shown as mean ± standard deviation. *$P$<0.05, **$P$<0.01, ***$P$<0.001, ****$P$<0.0001; NS: not significant ($P$>0.05). TCM: central memory T cell; NK: natural killer; IFN-γ: interferon-γ; M: macrophage.

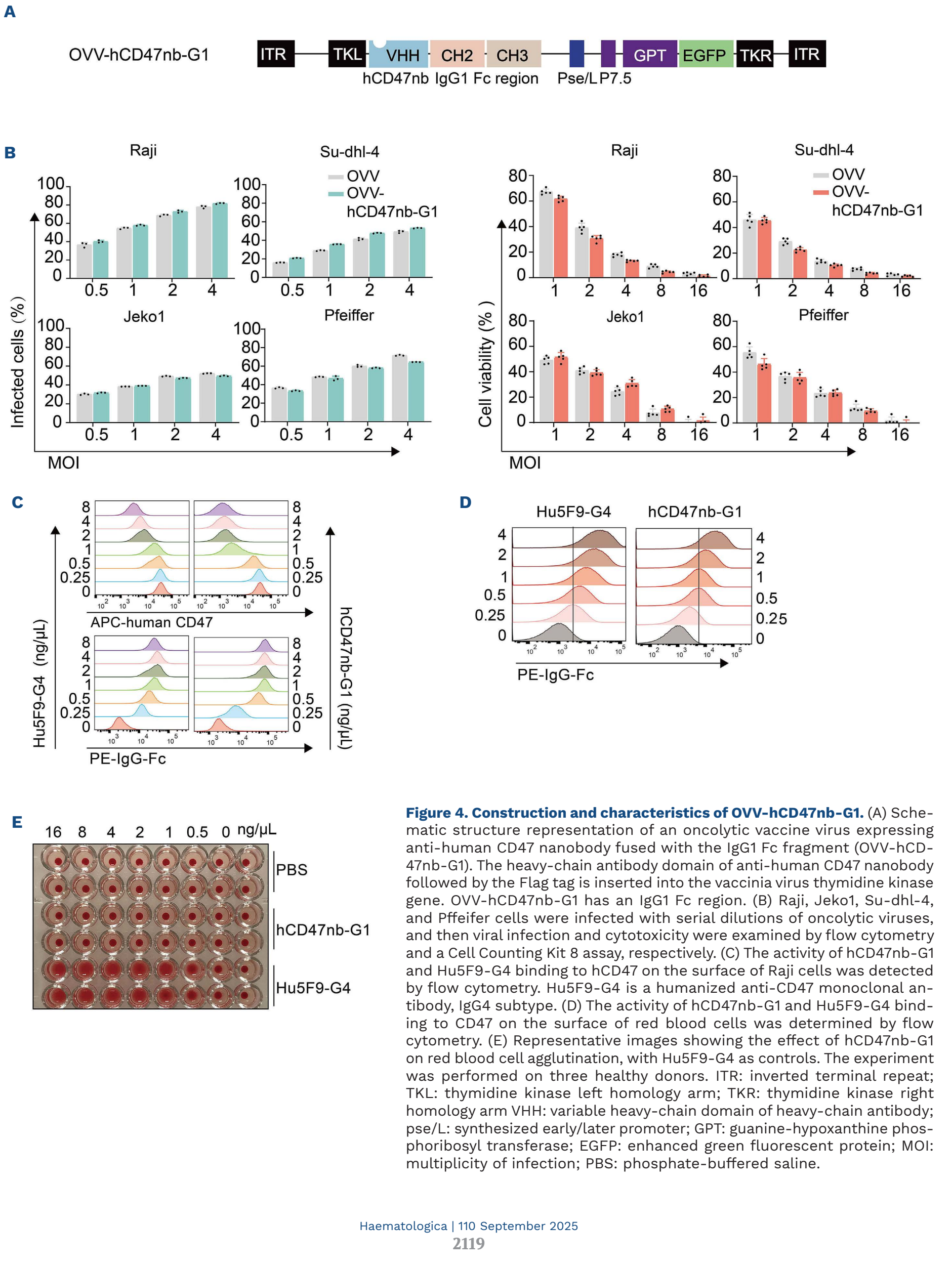


**Figure 4. Construction and characteristics of OVV-hCD47nb-G1.** (A) Schematic structure representation of an oncolytic vaccine virus expressing anti-human CD47 nanobody fused with the IgG1 Fc fragment (OVV-hCD47nb-G1). The heavy-chain antibody domain of anti-human CD47 nanobody followed by the Flag tag is inserted into the vaccinia virus thymidine kinase gene. OVV-hCD47nb-G1 has an IgG1 Fc region. (B) Raji, Jeko1, Su-dhl-4, and Pffeifer cells were infected with serial dilutions of oncolytic viruses, and then viral infection and cytotoxicity were examined by flow cytometry and a Cell Counting Kit 8 assay, respectively. (C) The activity of hCD47nb-G1 and Hu5F9-G4 binding to hCD47 on the surface of Raji cells was detected by flow cytometry. Hu5F9-G4 is a humanized anti-CD47 monoclonal antibody, IgG4 subtype. (D) The activity of hCD47nb-G1 and Hu5F9-G4 binding to CD47 on the surface of red blood cells was determined by flow cytometry. (E) Representative images showing the effect of hCD47nb-G1 on red blood cell agglutination, with Hu5F9-G4 as controls. The experiment was performed on three healthy donors. ITR: inverted terminal repeat; TKL: thymidine kinase left homology arm; TKR: thymidine kinase right homology arm VHH: variable heavy-chain domain of heavy-chain antibody; pse/L: synthesized early/later promoter; GPT: guanine-hypoxanthine phosphoribosyl transferase; EGFP: enhanced green fluorescent protein; MOI: multiplicity of infection; PBS: phosphate-buffered saline.

cells *in vitro*, as detected by western blot (*Online Supplementary Figure S2A*). The level of secretion of hCD47nb-G1 exhibited a dose- and time-dependent increase, correlating with viral dose and culture duration (*Online Supplementary Figure S2B*).

To evaluate CD47 targeting, Raji cells were treated with purified hCD47nb-G1 or Hu5F9-G4. Flow cytometry revealed dose-dependent reductions in CD47 surface expression and increased antibody binding (Figure 4C), confirming effective CD47 engagement.

We next investigated whether hCD47nb-G1 treatment elicited adverse effects on red blood cells. Interestingly, while both agents bound CD47 on red blood cells in a dose-dependent manner (Figure 4D), hCD47nb-G1 avoided hemagglutination, unlike Hu5F9-G4, which induced significant red blood cell clumping (Figure 4E), aligning with the reported toxicity of CD47 monoclonal antibodies.[25,26]

### *In vitro* activation of macrophages and natural killer cells mediated by hCD47nb-G1

To investigate the functional activity of hCD47nb-G1 secreted by OVV-hCD47nb-G1, we generated CD47-knockout (CD47-KO) Raji cells (*Online Supplementary Figure S3A*) and confirmed the lack of hCD47nb-G1 binding to CD47 on these KO tumor cells (*Online Supplementary Figure S3B, C*). Greater macrophage phagocytosis was observed not only in Raji cells upon anti-CD47 antibody and OVV-hCD47nb-G1 treatment, but also in CD47-KO Raji cells (Figure 5A, *Online Supplementary Figure S3D*). This effect of hCD47nb-G1 and Hu5F9-G4 was also demonstrated by confocal fluorescence microscopy analysis (Figure 5B).

The SIRPα-CD47 interaction suppresses key engulfment signals, particularly the SHP1/SHP2 signaling pathway.[27,28] We observed that CD47 KO in Raji cells and hCD47nb-G1 treatment inhibited SIRPα, increased total SHP-1 expression, and diminished SHP-1 activation. This ultimately led to the activation of STAT3, a downstream signaling component of SIRPα, in bone marrow-derived macrophages (*Online Supplementary Figure S3E*). hCD47nb-G1 treatment upregulated proinflammatory cytokines (*Il6*, *Il1β*, *Nos2*, *Ccl2*) and *Il10* while downregulating the M2 marker Mrc1 in bone marrow-derived macrophages (Figure 5C).

Given the OVV-induced NK cell infiltration and Fc receptor-mediated enhanced antitumor effects of anti-CD47 antibodies,[25,29] we examined NK cell activation by hCD47nb-G1 that contained IgG1 Fc fragment. A clear dose-dependent cytotoxic effect of NK cells obtained from three donors was validated by a 4 h co-culture in which increasing doses of hCD47nb-G1 were used (Figure 5D). The treatment significantly enhanced NK cell secretion of TNF-α, IFN-γ, and IL-10, along with increased CD107a expression indicating degranulation (Figure 5E).

### Superior therapeutic benefits and immune cell infiltration induced by OVV-hCD47nb-G1

We sought to confirm the interaction between these two therapeutic platforms. SCID mice bearing bilateral tumors received PBS, OVV, or OVV-hCD47nb-G1 via intratumoral injection in the right flank when tumors reached approximately 75 $mm^3$ (Figure 6A). While both OVV and OVV-hCD47nb-G1 suppressed ipsilateral tumor growth, only OVV-hCD47nb-G1 induced near-complete regression within 4 weeks. Contralateral tumors showed significant inhibition exclusively in the OVV-hCD47nb-G1 group (Figure 6B). Importantly, OVV-hCD47nb-G1 treatment significantly prolonged the survival of mice as compared with that of the animals in the PBS control and OVV treatment groups (Figure 6C), with no treatment-related weight loss (Figure 6D), or hematologic abnormalities (*Online Supplementary Figure S4A*). Correspondingly, elevated hCD47nb-G1 transcripts were detected only in OVV-hCD47nb-G1-treated ipsilateral tumors (*Online Supplementary Figure S4B*). Immunohistochemistry confirmed specific hCD47nb-G1 binding and vaccinia virus A27L protein expression in tumors of the right flank injected with viruses. Importantly, OVV-hCD47nb-G1 induced superior NK cell and macrophage infiltration compared to OVV in both injected (Figure 6E) and non-injected contralateral tumors, despite undetectable A27L and hCD47nb-G1 in the latter (Figure 6F).

Based on the immune cell infiltration induced by OVV-hCD47nb-G1 and the critical role of the tumor microenvironment in resistance to CAR T-cell therapy, we investigated whether OVV-hCD47nb-G1 could synergize with CAR T cells. For this purpose, NSG mice bearing subcutaneous Raji lymphoma xenografts were treated with OVV-hCD47nb-G1 via intratumoral injection, followed by administration of CD19 CAR T cells (Figure 7A). Tumors in mice treated with CD19 CAR T cells or the virus alone showed moderate regression, whereas tumors in the combination therapy group exhibited dramatically reduced growth (Figure 7B). Three days after viral injection, tumors from three randomly selected mice were excised. Flow cytometry and quantitative polymerase chain reaction analyses revealed significantly greater CAR T-cell infiltration in the combination therapy group compared to the CD19 CAR T-cell monotherapy group (Figure 7C, D).

### OVV-CD47nb-G1 enhances recruitment of immune cells and antitumor efficacy by secreting more chemokines *in vivo*

Eradicating systemic tumors is necessary for effective treatment of lymphomas. In order to study this aspect, we established a systemic tumor model by injecting Raji-luc cells into NSG mice. After 5 days, the mice were given OVV, or OVV-hCD47nb-G1 ($1\times10^7$ PFU) via intraperitoneal injection, and tumor growth was tracked using bioluminescence imaging (Figure 8A). Treatment with OVV-hCD47nb-G1 was much more effective, leading to almost complete tumor regression in three of four mice (Figure 8B). On day 14, mice receiving OVV or OVV-hCD47nb-G1 displayed an average weight loss of 10.63% (±9.25%) and 10.03% (±2.79%), respectively (Figure 8C). Forty-eight hours following the injection, peripheral blood mononuclear cells and serum were collected for fluorescence-activated

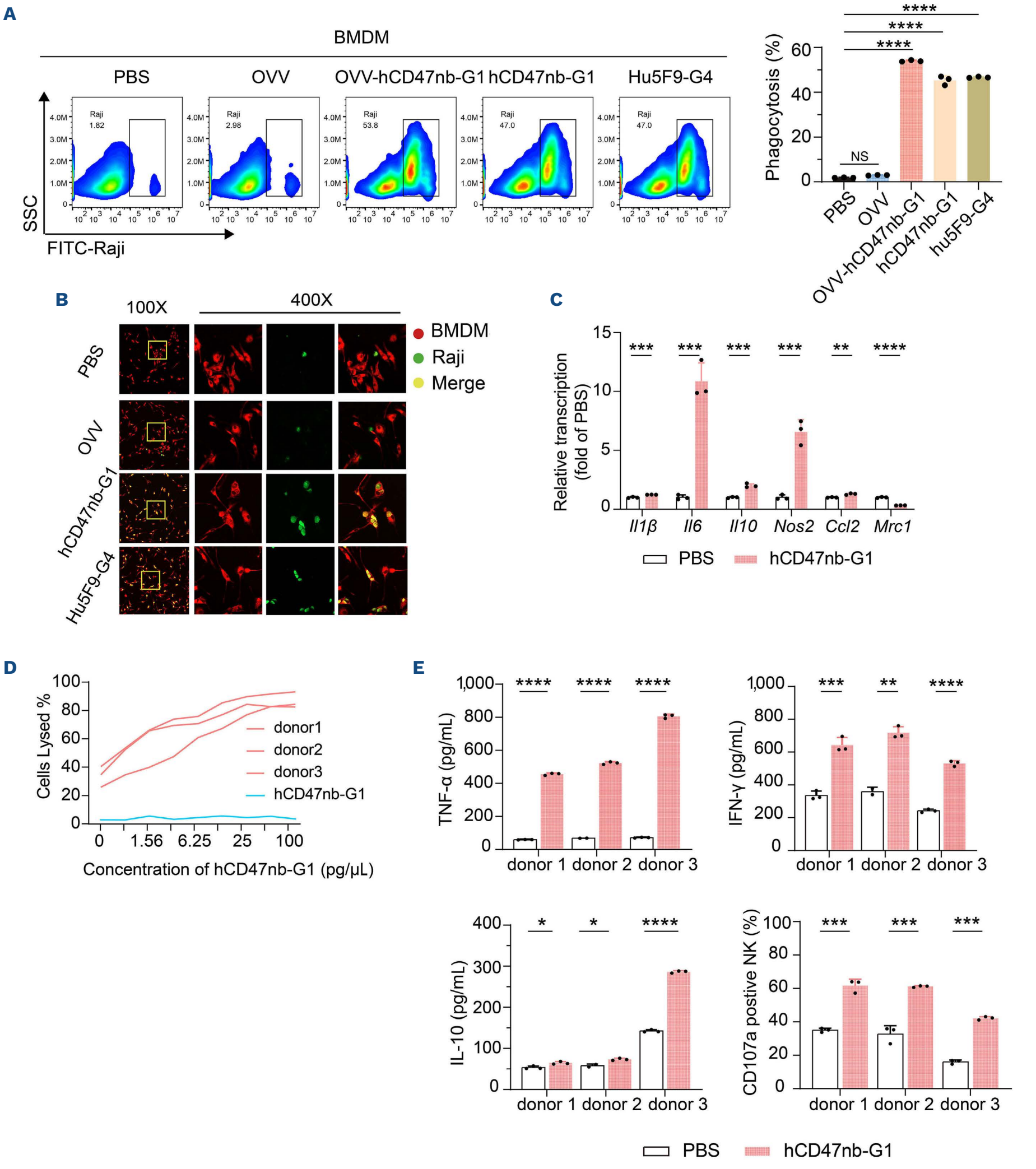


**Figure 5. hCD47nb-G1 activates stronger anti-tumor effects of macrophages and natural killer cells.** (A, B) The effects of supernatants of oncolytic vaccine virus (OVV), OVV expressing anti-human CD47 nanobody fused with the IgG1 Fc fragment (OVV-hCD47nb-G1), purified hCD47nb-G1 (5 ng/μL), and Hu5F9-G4 (5 ng/μL) on phagocytosis of Raji cells by bone marrow-derived macrophages (BMDM) using flow cytometry (A) and confocal fluorescence microscopy (B). The supernatants were harvested from cultures of Raji cells treated with viruses (4 multiplicity of infection) for 48 hours (h). (C) BMDM were co-cultured with Raji cells at a ratio

Continued on following page.

of 2:1 with or without 5 ng/μL hCD47nb-G1 for 24 h, and then adhered BMDM were collected for quantitative reverse transcription polymerase chain reaction analysis. (D) Raji cells were co-cultured with human natural killer (NK) cells at a ratio of 3:1 in the presence of different concentrations of hCD47nb-G1 for 4 h, and then the cytotoxicity of NK cells was evaluated by a luciferase-based cytotoxicity assay. (E) The levels of tumor necrosis factor-α, interferon-γ, and interleukin-10 in the supernatants of co-cultures of NK cells and Raji were determined using Cytometric Beads Array, and the frequency of $CD107a^+$ $CD56^+$ NK cells was also detected by flow cytometry. Comparisons were made using one-way analysis of variance with Tukey's multiple comparison tests. All data are shown as mean ± standard deviation. **P*<0.05, ***P*<0.01, ****P*<0.001, *****P*<0.0001; NS: not statistically significant (*P*>0.05). SSC: side scatter; PBS: phosphate-buffered saline; TNF-α: tumor necrosis factor-α; IFN-γ: interferon-γ; IL-10: interleukin-10.

cell sorting and Luminex analysis. These analyses were conducted to assess the binding of hCD47nb-G1 on tumor cells *in vivo* and changes in cytokine and chemokine levels. In mice treated with OVV-hCD47nb-G1, 21.74% (±11.49%) of Raji cells were hCD47nb-G1-positive. (Figure 8D).

Heatmap analysis showed that mice administered OVV-hCD47nb-G1 had a distinct cytokine and chemokine expression profile (Figure 8E). Serum levels of IL-2, IL-6, IL-10, CXC motif chemokine ligand (CXCL)1, CXCL10, CXCL12, CC motif chemokine ligand (CCL)3, CCL4, CCL7, CCL17, and CCL19 were significantly elevated in mice treated with OVV-hCD47nb-G1 compared to those receiving OVV or PBS. Compared with the PBS control, there was a significantly higher level of granulocyte-macrophage colony-stimulating factor and several chemokines, including CXCL5, CXCL11, CXCL13, CCL5, and CCL12, associated with the OVV-hCD47nb-G1 treatment, whereas OVV treatment only raised the levels of CXCL10 and CXCL12 (Figure 8F).

We next investigated the superiority of OVV-hCD47nb-G1 over existing CD47-targeted therapies such as Hu5F9-G4 in terms of safety and efficacy. NSG mice bearing Raji cell xenografts were treated with Hu5F9, OVV, and OVV-hCD47nb-G1 via intraperitoneal injection (*Online Supplementary Figure S5A*). The results demonstrated that OVV-hCD47nb-G1 exhibited superior antitumor activity compared to both Hu5F9 and OVV (*Online Supplementary Figure S5B*), which translated into significantly prolonged survival (*Online Supplementary Figure S5C*). Notably, while both therapeutic agents showed inhibition of hemoglobin, mice treated with OVV-hCD47nb-G1 displayed a less pronounced decrease in hemoglobin levels compared to those receiving Hu5F9 (127.4±4.037 g/L *vs*. 120.6±4.336 g/L; *P*=0.0438). Additionally, Hu5F9 treatment was associated with reduced white blood cell counts (*Online Supplementary Figure S5D*). Viral tracking through A56R expression revealed detectable levels in the liver, spleen, lungs, and bone marrow of virus-treated mice (*Online Supplementary Figure S5E*).

## Discussion

High CD47 expression correlates with poor survival in newly diagnosed DLBCL patients treated with R-CHOP, an effect related to genomic alterations and an immunosuppressive tumor microenvironment.[8,9] Here we show that CD47 is also a strong adverse prognostic biomarker in relapsed/refractory DLBCL patients who received CD19-specific CAR T-cell treatment.

Blockade of the CD47/SIRPα axis has been shown to enhance anti-B-cell lymphoma activities,[30-32] thus representing a pillar for lymphoma immunotherapy either on its own or integrated with other therapies. Currently, various combination treatments including anti-CD47 antibodies are being investigated in clinical trials.[33] A pilot study investigating Hu5F9-G4 in combination with rituximab (H + R) for treating B-cell non-Hodgkin lymphoma demonstrated excellent results. The synergistic mechanism involves the Fc region of rituximab, which enhances macrophage activity by providing a potent pro-phagocytic signal through stimulation of antibody-dependent cellular phagocytosis.[14] Three-year follow-up of this phase Ib/II study showed that complete response occurred in 12.1% (12/99) of DLBCL patients who received H + R. Furthermore, the complete response rate was 39% in 33 patients treated with H + R plus gemcitabine-oxaliplatin, indicating that this regimen has clinical activity.[34] However, anemia and thrombocytopenia were common adverse events, which might result in low tolerated doses in clinical studies or treatment discontinuation, thereby limiting the effects of these treatments on the tumor.

Oncolytic viruses selectively target and destroy cancer cells while largely sparing normal cells. This specificity arises from their ability to exploit unique features of cancer biology, such as defective antiviral signaling or dysregulated growth pathways. Furthermore, oncolytic viruses stimulate innate immunity and convert immunologically "cold" tumors (characterized by minimal immune infiltration) into "hot" tumors by enhancing immune cell recruitment (e.g., T cells, NK cells) and activating antitumor adaptive immunity. These dual mechanisms – direct oncolysis and immune modulation – position oncolytic viruses as compelling candidates for combination cancer immunotherapy.[16-18] Instead of combination treatment, encoding checkpoint antibodies including anti-CD47 antibody by oncolytic viruses increases local concentrations within the tumor microenvironment while decreasing systemic exposure.[23,35] In this study, we first engineered an OVV expressing an anti-mouse CD47 nanobody (OVV-mCD47nb). This construct directly lyses lymphoma cells through oncolytic activity and indirectly enhances macrophage-mediated phagocytosis via secreted nanobodies.

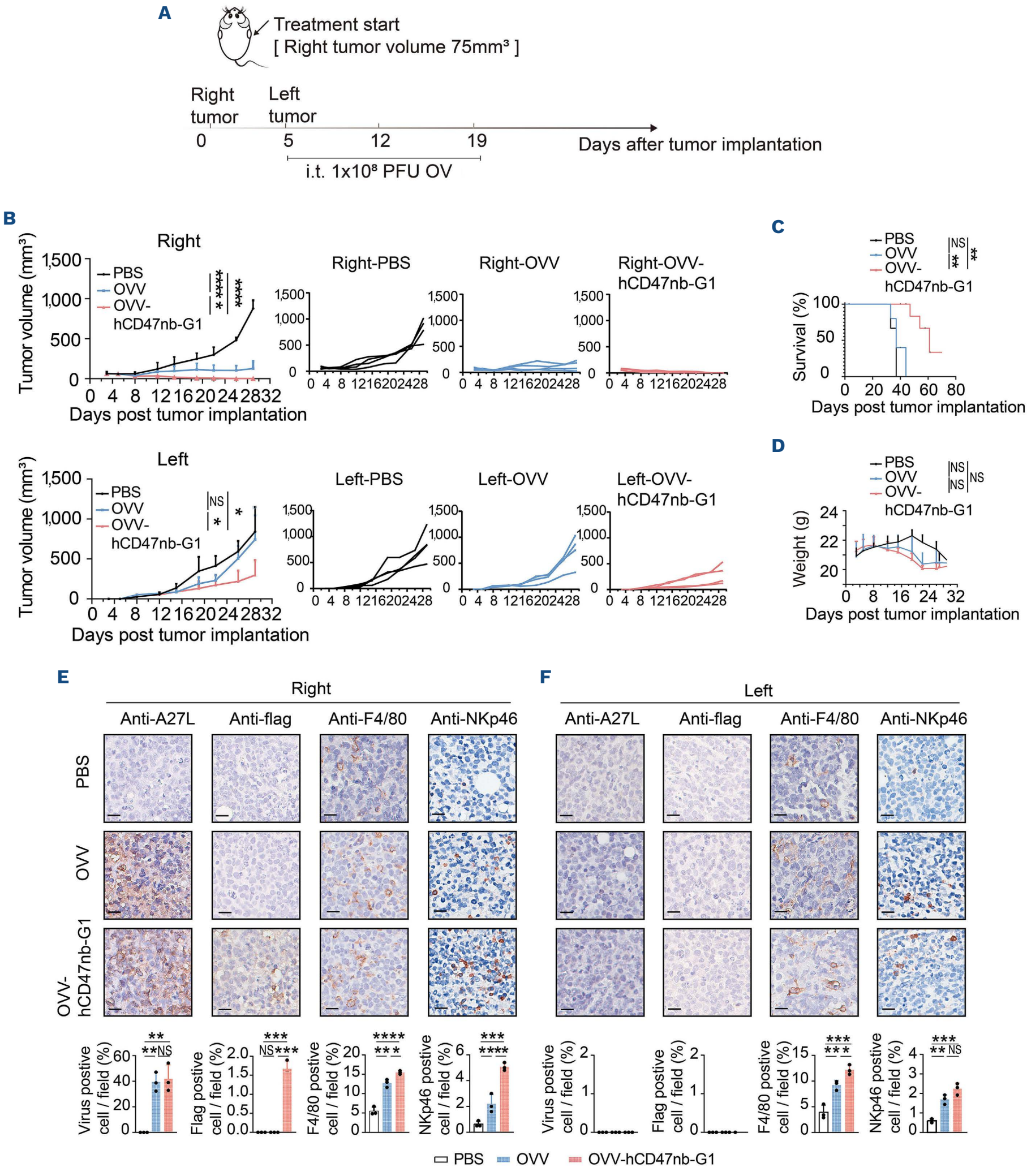


**Figure 6. OVV-hCD47nb-G1 improves therapeutic efficacy against B-cell lymphoma *in vivo*.** (A) SCID mice were inoculated with 5×10$^6$ Raji cells in the right flank on day 0 and the left flank on day 5. When the tumors of the right flank reached approximately 75 mm$^3$, mice (N=4) were intratumorally injected with phosphate-buffered saline, 1×10$^8$ plaque-forming units of oncolytic virus vaccine (OVV), and OVV expressing anti-human CD47 nanobody fused with the IgG1 Fc fragment (OVV-hCD47nb-G1) once a week for a total of three time. (B) Tumors in the right and left flanks were measured at the indicated times and calculated volumes are presented as growth

Continued on following page.

curves. (C) Kaplan-Meier survival curves for Raji tumor-bearing mice. (D) Mouse body weight was monitored at the indicated times. (E, F) Immunohistochemistry analysis of bilateral tumors was performed. Representative images are shown. Scale bars, 25 μm. Comparisons were made using one-way analysis of variance with Tukey's multiple comparison tests (B and D) on day 29, (E and F) on day 14, and the log-rank (Mantel-Cox) test (C). All data are shown as mean ± standard deviation. **P*<0.05, ***P*<0.01, ****P*<0.001, *****P*<0.0001; NS: not statistically significant (*P*>0.05). PFU: plaque-forming units; OV: oncolytic viruses; PBS: phosphate-buffered saline.

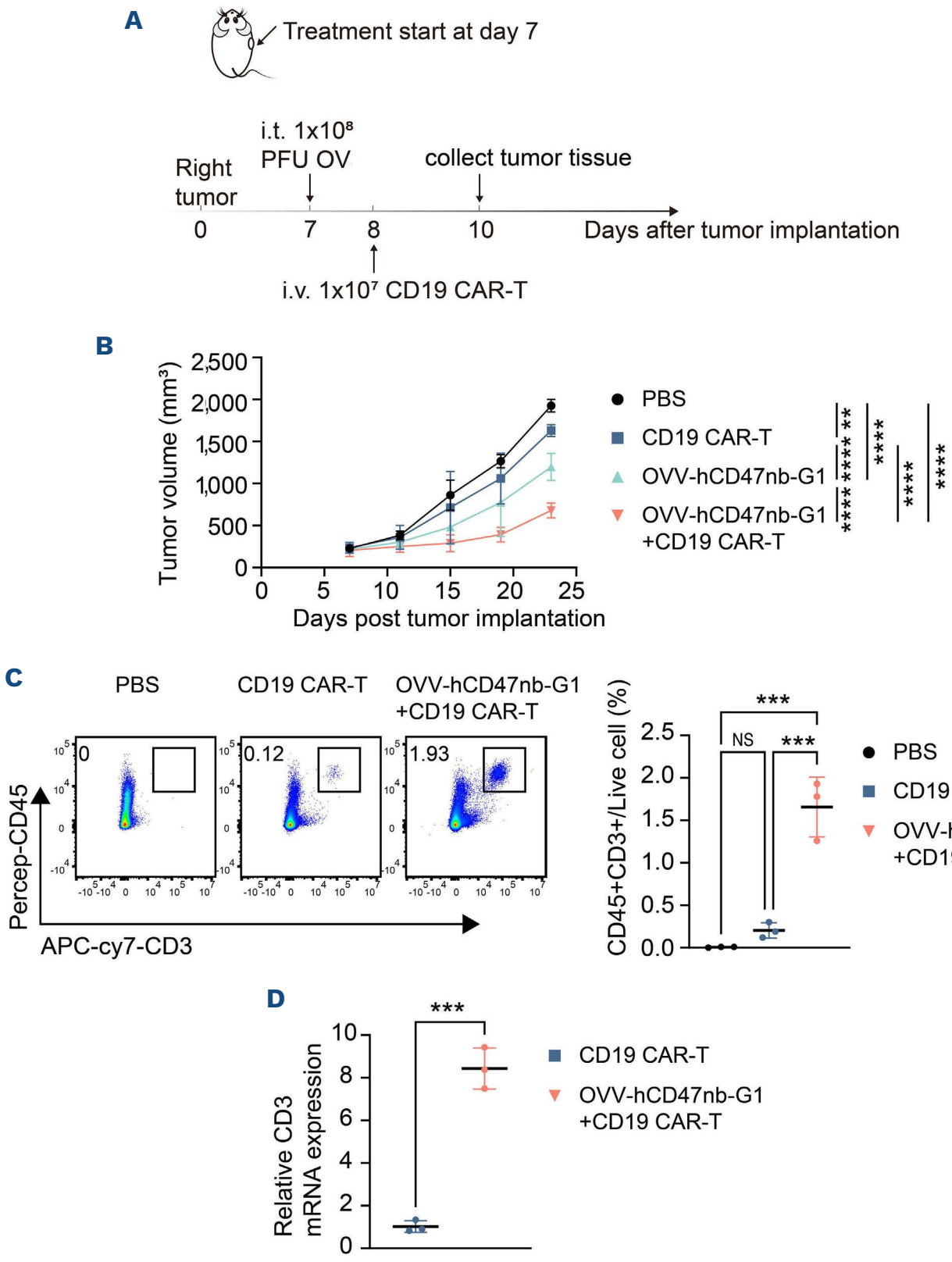


**Figure 7. Synergistic effect of OVV-hCD47nb-G1 and CD19-specific chimeric antigen receptor T cells.** (A) Treatment timeline. NSG mice were subcutaneously inoculated with 5x10⁶ Raji cells. On day 7, the mice received intratumoral administration of 1×10⁸ plaque-forming units of oncolytic vaccine virus expressing anti-human CD47 nanobody fused with the IgG1 Fc fragment (OVV-hCD47nb-G1), followed by intravenous injection of 1×10⁷ CD19 chimeric antigen receptor T cells or phosphate-buffered saline control 24 hours later. Tumor tissues were harvested on day 10 for quantitative reverse transcription polymerase chain reaction and flow cytometry analysis (N=3). (B) Tumor volume dynamics. Average tumor volume in lymphoma-bearing mice across treatment groups (N=5). (C) Immune cell infiltration in the tumor microenvironment. Representative flow cytometry plots of $CD45^{+}CD3^{+}$ cells stained with anti-human CD45 and CD3 antibodies. (D) CD3 mRNA expression in tumors. Relative CD3 mRNA level in tumors treated with CD19 chimeric antigen receptor T cells alone or in combination with OVV-hCD47nb-G1. Data were analyzed by one-way analysis of variance with Tukey's *post hoc* (multiple comparisons) test or Student's *t* test (two-group comparison). **P*<0.05, ***P*<0.01, ****P*<0.001, *****P*<0.0001, NS: not statistically significant. All values represent mean ± standard deviation. i.t.: intratumoral; PFU: plaque-forming units; OV: oncolytic virus; i.v.: intravenous; CAR: chimeric antigen receptor; PBS: phosphate-buffered saline.

To facilitate clinical translation, we further developed a humanized version of this platform: an OVV expressing an anti-human CD47 nanobody fused with the IgG1 Fc fragment (OVV-hCD47nb-G1). The hCD47nb fusion protein not only potentiates macrophage activity but also engages NK cells, thereby amplifying antilymphoma immunity. Notably, unlike Hu5F9-G4, which induces hemagglutination, hCD47nb-G1 binds to red blood cells without causing significant agglutination, despite sharing similar red blood cell-binding properties. While the mechanism underlying this differential effect remains unclear and warrants further investigation, our finding aligns with prior reports on SRF231, a clinical-stage human anti-CD47 antibody that exhibits antitumor efficacy without triggering red blood cell phagocytosis or agglutination.[36] Intratumoral administration of OVV-hCD47nb-G1 in a mouse model was well tolerated, with no significant reduction in red blood cell counts or hemoglobin. In contrast, systemic delivery, via intraperitoneal injection, of both OVV-hCD47nb-G1 and Hu5F9 significantly decreased hemoglobin levels compared to those in PBS-treated controls. Notably, the reduction in hemoglobin in the OVV-hCD47nb-G1 group was less pronounced than that caused by Hu5F9. These findings indicate that OVV-hCD47nb-G1 represents a novel, potent, and safe anti-CD47 combination therapy for lymphoma, leveraging synergistic antitumor activity while mitigating systemic hematologic toxicity associated with conventional CD47-targeting agents.

The heterogeneous composition of the tumor microenvironment critically influences DLBCL progression, with specific immune subsets dictating clinical outcomes.[37,38] Reduced T-cell infiltration correlates with disease advancement,[39] while low $CD8^+$ T-cell prevalence and elevated CD4/CD8 ratios predict poor survival.[40] Prognosis further depends on T-cell activation status, as patients with diminished $CD3^+$ T cells and $PD1^+$ $CD4^+/CD8^+$ cell populations exhibit shorter survival.[41] Tumor-associated macrophages demonstrate phenotype-specific impacts: M2 polarization associates with inferior survival, contrasting with context-dependent M1 effects.[42] In our study, OVV or OVV-mCD47nb treatment significantly increased infiltration of macrophages and NK cells with macrophage polarization to the M1 phenotype and activation of NK cells. Interestingly, only OVV-mCD47nb significantly improved the infiltration of T cells in tumors, expanding $CD8^+$ T cells while decreasing the $CD4^+$ T-cell population. More importantly, OVV-hCD47nb-G1 exhibited robust antitumor activity against B-cell lymphoma across bilateral subcutaneous xenograft and systemic tumor models. In the bilateral tumor model, activated NK cells and macrophage infiltration increased in both OVV-hCD47nb-G1- and OVV-treated tumors and distant subcutaneous tumors, with OVV-hCD47nb-G1 showing stronger biological effects than OVV. These effects suggest that intratumoral virotherapy elicited a systemic immune response.

The remodeling of the tumor microenvironment by OVV-hCD-47nb-G1 might enhance the efficacy of CAR T-cell therapy. In this study, we demonstrated that combining OVV-hCD-47nb-G1 with CD19 CAR T cells not only improved therapeutic outcomes in subcutaneous lymphoma models but also overcame a critical barrier by significantly enhancing CAR T-cell tumor infiltration. The strategy represents a promising advance in cancer immunotherapy, warranting further investigation.

Chemokines, chemotactic cytokines regulating immune cell activation, migration, and function, play dual roles in pro- and anti-tumor responses.[43,44] An important finding of this study was that intraperitoneal administration of OVV-hCD-47nb-G1 induced a serum chemokine profile distinct from that induced by OVV, with broader chemokine upregulation. Among them, CCL2 and CCL4 were reported to be upregulated by the anti-CD47 IgG1 monoclonal antibody secreted by oncolytic viruses.[45] Oncolytic viruses armed with CCL5 or CXCL10 enhanced NK cell accumulation in tumor lesions and recruited $CXCR3^+$ T cells into the tumor microenvironment.[46] Similarly, CCL19-expressing OVV increased infiltration of T cells and dendritic cells into tumors.[47] Furthermore, intratumoral delivery of CXCL11-expressing oncolytic viruses not only elevated local $CD8^+$ T-cell numbers but also triggered a systemic rise in tumor-specific IFN-γ-producing $CD8^+$ T cells in the spleen and lymphoid organs.[48] Collectively, these findings suggest that the ability of OVV-hCD47nb-G1 to induce chemokine release may underlie its efficacy as a cancer immunotherapy.

Systemic delivery of oncolytic viruses is necessary for effective targeting of metastatic cancers.[49,50] In this study, we employed immunodeficient NSG mice to evaluate the therapeutic efficacy of intraperitoneal OVV-hCD47nb-G1 administration. While this model demonstrated antitumor activity, its inability to effectively clear residual virus post-treatment highlights the need for humanized mouse models to investigate therapeutic outcomes under immune-competent conditions in which rapid viral clearance can occur. Furthermore, clinical translation of OVV-hCD-47nb-G1 faces additional safety challenges, particularly therapy-related adverse events such as toxicity mediated by chemokine hyperactivation.

In summary, we have developed an OVV-based platform capable of local and systemic delivery of an anti-human CD47 nanobody fused with the IgG1 Fc fragment (hCD-47nb-G1) that lacks hemagglutination properties for B-cell lymphoma therapy. This multifunctional platform drives antitumor responses through four synergistic mechanisms: including direct oncolysis of tumor cells, Fc-mediated enhancement of innate immune cell cytotoxicity, recruitment and activation of both innate and adaptive immune cells, and immune checkpoint modulation in macrophages. By integrating these features, our platform could overcome key limitations of anti-CD47 monoclonal antibodies or conventional OVV therapies, demonstrating translational potential for improved clinical outcomes in B-cell lymphomas.

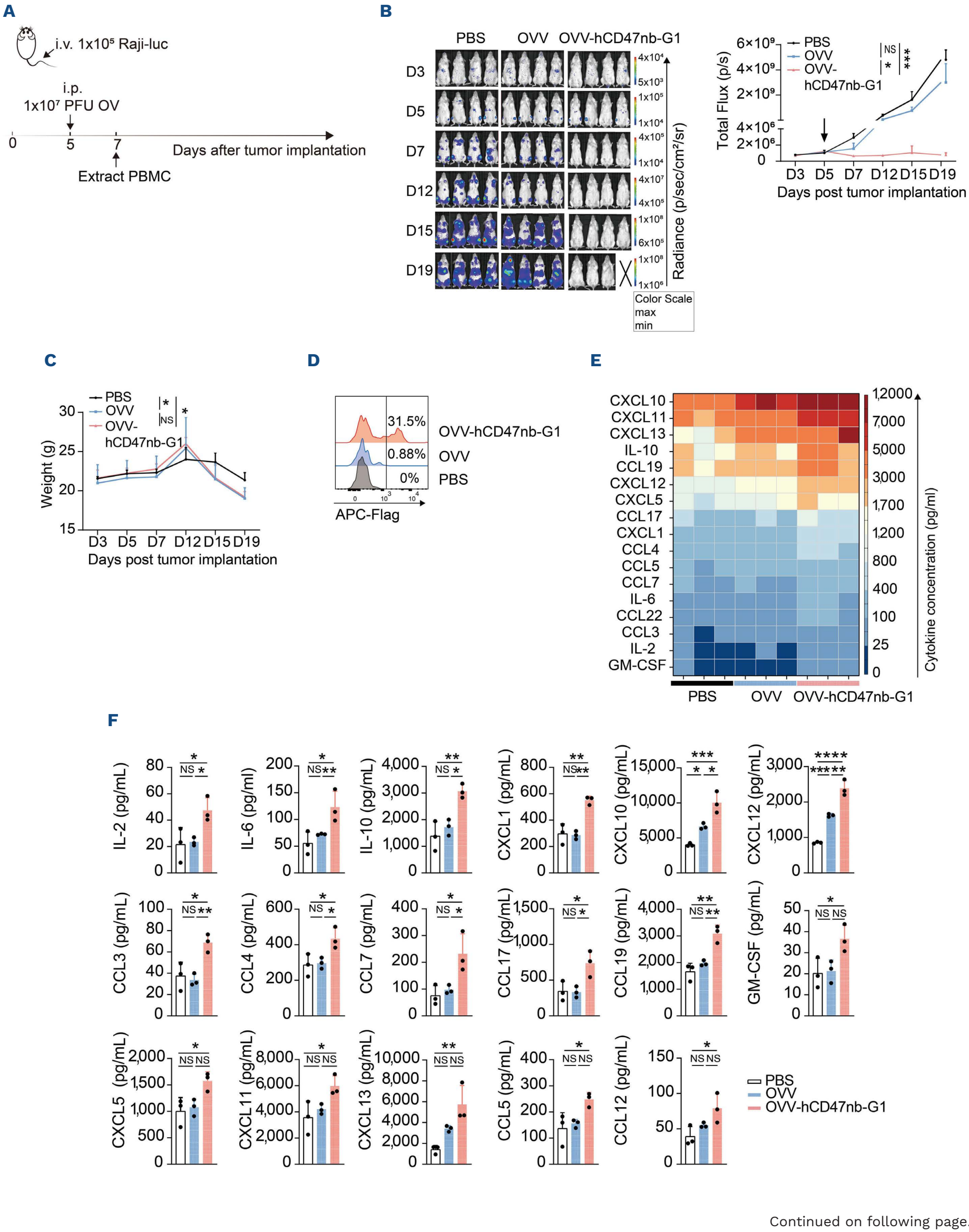


Continued on following page.

**Figure 8. OVV-CD47-G1 enhances the recruitment of immune cells and antitumor efficacy by secreting more chemokines *in vivo*.** (A) Experimental design: NSG mice were injected intravenously with Raji cells. At day 5, mice were randomly assigned to receive phosphate-buffered saline, oncolytic vaccine virus (OVV), or OVV expressing anti-human CD47 nanobody fused with the IgG1 Fc fragment (OVV-hCD47nb-G1) ($1\times10^7$ plaque-forming units/mice, intraperitoneal injection) (N=4). (B) Luciferase activity of Raji-luc cells was analyzed by bioluminescence imaging at the indicated day until day 19 (N=4). (C) Mouse body weight was monitored at the indicated times. (D) At day 7, peripheral blood mononuclear cells were collected for analysis of hCD47nb-G1 binding on the surface of Raji cells *in vivo*. (E) The heatmap demonstrates a distinct cytokine and chemokine expression profile in the OVV-hCD-47nb-G1 group. (F) Serum levels of cytokines and chemokines in animals treated with phosphate-buffered saline, OVV and OVV-hCD47nb-G1. **P*<0.05, ***P*<0.01, ****P*<0.001, *****P*<0.0001; NS: not statistically significant (*P*>0.05). Comparisons were made using one-way analysis of variance with Tukey's multiple comparisons and Student's *t* test. All data are shown as mean ± standard deviation. i.v.: intravenous; i.p.: intraperitoneal; PFU: plaque-forming units; OV: oncolytic viruses; PBMC: peripheral blood mononuclear cells; PBS: phosphate-buffered saline; CXCL: CXC motif chemokine ligand; IL: interleukin; CCL: CC motif chemokine ligand; GM-CSF: granulocyte-macrophage colony-stimulating factor.

## Disclosures

*No conflicts of interest to disclose.*

## Contributions

*WQ and WL designed the study. ML, YZ, LZ, MZ and SW performed in vitro and in vivo studies. ML and WQ analyzed and interpreted data, and drafted the manuscript. All authors read the final manuscript, provided feedback throughout the development process, and approved the final submitted version.*

## Funding

*This work was supported by funds from the National Natural Science Foundation of China (N. 82350104), the Noncommunicable Chronic Diseases-National Science and Technology Major Project (N. 2023ZD0501300), the Science Technology Department of Zhejiang Province (N. 2021C03117), and Zhejiang Provincial Natural Science Foundation of China (N. LY24H080001).*

## Data-sharing statement

*The original contributions presented in the study are included in the article or Online Supplementary Material. Further inquiries can be directed to the authors for correspondence.*

# References

1. Siegel RL, Miller KD, Wagle NS, Jemal A. Cancer statistics, 2023. CA Cancer J Clin. 2023;73(1):17-48.
2. Crump M, Neelapu SS, Farooq U, et al. Outcomes in refractory diffuse large B-cell lymphoma: results from the international SCHOLAR-1 study. Blood. 2017;130(16):1800-1808.
3. Locke FL, Ghobadi A, Jacobson CA, et al. Long-term safety and activity of axicabtagene ciloleucel in refractory large B-cell lymphoma (ZUMA-1): a single-arm, multicentre, phase 1-2 trial. Lancet Oncol. 2019;20(1):31-42.
4. Westin JR, Kersten MJ, Salles G, et al. Efficacy and safety of CD19‐directed CAR‐T cell therapies in patients with relapsed/refractory aggressive B‐cell lymphomas: observations from the JULIET, ZUMA‐1, and TRANSCEND trials. Am J Hematol. 2021;96(10):1295-1312.
5. Sterner RC, Sterner RM. CAR-T cell therapy: current limitations and potential strategies. Blood Cancer J. 2021;11(4):69.
6. Ansell SM, Lin Y. Immunotherapy of lymphomas. J Clin Invest. 2020;130(4):1576-1585.
7. Feng M, Jiang W, Kim BYS, Zhang CC, Fu Y-X, Weissman IL. Phagocytosis checkpoints as new targets for cancer immunotherapy. Nat Rev Cancer. 2019;19(10):568-586.
8. Shen Y-G, Ji M-M, Yi H-M, et al. CD47 overexpression is related to tumour-associated macrophage infiltration and diffuse large B-cell lymphoma progression. Clin Transl Med. 2024;14(1):e1532.
9. Bouwstra R, He Y, Boer J, et al. CD47 expression defines efficacy of rituximab with CHOP in non-germinal center B-cell (non-GCB) diffuse large B-cell lymphoma patients (DLBCL), but not in GCB DLBCL. Cancer Immunol Res. 2019;7(10):1663-1671.
10. Kazama R, Miyoshi H, Takeuchi M, et al. Combination of CD47 and signal-regulatory protein-α constituting the "don't eat me signal" is a prognostic factor in diffuse large B-cell lymphoma. Cancer Sci. 2020;111(7):2608-2619.
11. Cho J, Yoon SE, Kim SJ, Ko YH, Kim WS. CD47 overexpression is common in intestinal non-GCB type diffuse large B-cell lymphoma and associated with 18q21 gain. Blood Adv. 2022;6(24):6120-6130.
12. Yang H, Xun Y, You H. The landscape overview of CD47-based immunotherapy for hematological malignancies. Biomark Res. 2023;11(1):15.
13. Lentz RW, Colton MD, Mitra SS, Messersmith WA. Innate immune checkpoint inhibitors: the next breakthrough in medical oncology? Mol Cancer Ther. 2021;20(6):961-974.
14. Advani R, Flinn I, Popplewell L, et al. CD47 blockade by Hu5F9-G4 and rituximab in non-Hodgkin's lymphoma. N Engl J Med. 2018;379(18):1711-1721.
15. Bouwstra R, van Meerten T, Bremer E. CD47-SIRPα blocking-based immunotherapy: current and prospective therapeutic strategies. Clin Transl Med. 2022;12(8):e943.
16. Tian Y, Xie D, Yang L. Engineering strategies to enhance oncolytic viruses in cancer immunotherapy. Signal Transduct Target Ther. 2022;7(1):117.
17. Lin C, Teng W, Tian Y, Li S, Xia N, Huang C. Immune landscape and response to oncolytic virus-based immunotherapy. Front Med. 2024;18(3):411-429.
18. Wang L, Chard Dunmall LS, Cheng Z, Wang Y. Remodeling the tumor microenvironment by oncolytic viruses: beyond oncolysis of tumor cells for cancer treatment. J Immunother Cancer. 2022;10(5):e004167.

19. Zuo S, Wei M, Xu T, et al. An engineered oncolytic vaccinia virus encoding a single-chain variable fragment against TIGIT induces effective antitumor immunity and synergizes with PD-1 or LAG-3 blockade. J Immunother Cancer. 2021;9(12):e002843.
20. Passaro C, Alayo Q, Laura I, et al. Arming an oncolytic herpes simplex virus type 1 with a single-chain fragment variable antibody against PD-1 for experimental glioblastoma therapy. Clin Cancer Res. 2019;25(1):290-299.
21. Lei W, Ye Q, Hao Y, et al. CD19-targeted BiTE expression by an oncolytic vaccinia virus significantly augments therapeutic efficacy against B-cell lymphoma. Blood Cancer J. 2022;12(2):35.
22. Wang G, Kang X, Chen KS, et al. An engineered oncolytic virus expressing PD-L1 inhibitors activates tumor neoantigen-specific T cell responses. Nat Commun. 2020;11(1):1395.
23. Tian L, Xu B, Teng K-Y, et al. Targeting Fc receptor-mediated effects and the "don't eat me" signal with an oncolytic virus expressing an anti-CD47 antibody to treat metastatic ovarian cancer. Clin Cancer Res. 2022;28(1):201-214.
24. Vogel DYS, Glim JE, Stavenuiter AWD, et al. Human macrophage polarization in vitro: maturation and activation methods compared. Immunobiology. 2014;219(9):695-703.
25. Ma L, Zhu M, Gai J, et al. Preclinical development of a novel CD47 nanobody with less toxicity and enhanced anti-cancer therapeutic potential. J Nanobiotechnology. 2020;18(1):12.
26. Pietsch EC, Dong J, Cardoso R, et al. Anti-leukemic activity and tolerability of anti-human CD47 monoclonal antibodies. Blood Cancer J. 2017;7(2):e536.
27. Hara K, Senga T, Biswas MHU, et al. Recovery of anoikis in Src-transformed cells and human breast carcinoma cells by restoration of the SIRP α1/SHP-2 signaling system. Cancer Res. 2011;71(4):1229-1234.
28. Shen Q, Zhao L, Pan L, et al. Soluble SIRP-alpha promotes murine acute lung injury through suppressing macrophage phagocytosis. Front Immunol. 2022;13:865579.
29. Osorio JC, Smith P, Knorr DA, Ravetch JV. The antitumor activities of anti-CD47 antibodies require Fc-FcgammaR interactions. Cancer Cell. 2023;41(12):2051-2065.e6.
30. Chao MP, Alizadeh AA, Tang C, et al. Anti-CD47 antibody synergizes with rituximab to promote phagocytosis and eradicate non-Hodgkin lymphoma. Cell. 2010;142(5):699-713.
31. Cao X, Wang Y, Zhang W, et al. Targeting macrophages for enhancing CD47 blockade-elicited lymphoma clearance and overcoming tumor-induced immunosuppression. Blood. 2022;139(22):3290-3302.
32. Biedermann A, Patra-Kneuer M, Mougiakakos D, et al. Blockade of the CD47/SIRPα checkpoint axis potentiates the macrophage-mediated anti-tumor efficacy of tafasitamab. Haematologica. 2024;109(12):3928-3940.
33. Zhao P, Xie L, Yu L, Wang P. Targeting CD47-SIRPα axis for Hodgkin and non-Hodgkin lymphoma immunotherapy. Genes Dis. 2024;11(1):205-217.
34. Maakaron JE, Asch A, Popplewell L, et al. Magrolimab plus rituximab with/without chemotherapy in patients with relapsed/refractory diffuse large B-cell lymphoma. Blood Adv. 2024;8(22):5864-5874.
35. Xu B, Tian L, Chen J, et al. An oncolytic virus expressing a full-length antibody enhances antitumor innate immune response to glioblastoma. Nat Commun. 2021;12(1):5908.
36. Peluso MO, Adam A, Armet CM, et al. The fully human anti-CD47 antibody SRF231 exerts dual-mechanism antitumor activity via engagement of the activating receptor CD32a. J Immunother Cancer. 2020;8(1):e000413.
37. Autio M, Leivonen S-K, Brück O, et al. Immune cell constitution in the tumor microenvironment predicts the outcome in diffuse large B-cell lymphoma. Haematologica. 2021;106(3):718-729.
38. Cerchietti L. Genetic mechanisms underlying tumor microenvironment composition and function in diffuse large B-cell lymphoma. Blood. 2024;143(12):1101-1111.
39. Guan X, Wang Y, Fang T, et al. Lymphoma cell-driven IL-16 is expressed in activated B-cell-like diffuse large B-cell lymphomas and regulates the pro-tumor microenvironment. Haematologica. 2024;110(2):425-438.
40. Chen Z, Deng X, Ye Y, et al. Novel risk stratification of de novo diffuse large B cell lymphoma based on tumour-infiltrating T lymphocytes evaluated by flow cytometry. Ann Hematol. 2019;98(2):391-399.
41. Colombo AR, Hav M, Singh M, et al. Single-cell spatial analysis of tumor immune architecture in diffuse large B-cell lymphoma. Blood Adv. 2022;6(16):4675-4690.
42. Koumpis E, Papoudou-Bai A, Papathanasiou K, Kolettas E, Kanavaros P, Hatzimichael E. Unraveling the immune microenvironment in diffuse large B-cell lymphoma: prognostic and potential therapeutic implications. Curr Issues Mol Biol. 2024;46(7):7048-7064.
43. Ozga AJ, Chow MT, Luster AD. Chemokines and the immune response to cancer. Immunity. 2021;54(5):859-874.
44. Mempel TR, Lill JK, Altenburger LM. How chemokines organize the tumour microenvironment. Nat Rev Cancer. 2024;24(1):28-50.
45. Wang J, Tian L, Barr T, et al. Enhanced treatment of breast cancer brain metastases with oncolytic virus expressing anti-CD47 antibody and temozolomide. Mol Ther Oncol. 2024;32(3):200824.
46. Li F, Sheng Y, Hou W, et al. CCL5-armed oncolytic virus augments CCR5-engineered NK cell infiltration and antitumor efficiency. J Immunother Cancer. 2020;8(1):e000131.
47. Li J, O'Malley M, Sampath P, Kalinski P, Bartlett DL, Thorne SH. Expression of CCL19 from oncolytic vaccinia enhances immunotherapeutic potential while maintaining oncolytic activity. Neoplasia. 2012;14(12):1115-1121.
48. Liu Z, Ravindranathan R, Li J, Kalinski P, Guo ZS, Bartlett DL. CXCL11-armed oncolytic poxvirus elicits potent antitumor immunity and shows enhanced therapeutic efficacy. Oncoimmunology. 2016;5(3):e1091554.
49. Russell SJ, Federspiel MJ, Peng K-W, et al. Remission of disseminated cancer after systemic oncolytic virotherapy. Mayo Clin Proc. 2014;89(7):926-933.
50. Shen W, Patnaik MM, Ruiz A, Russell SJ, Peng K-W. Immunovirotherapy with vesicular stomatitis virus and PD-L1 blockade enhances therapeutic outcome in murine acute myeloid leukemia. Blood. 2016;127(11):1449-1458.